A Warped Accretion Disk and Wide#Angle Outflow in the Inner Parsec of the Circinus Galaxy

A Warped Accretion Disk and Wide Angle Outflow in the Inner Parsec of the Circinus Galaxy

L. J. Greenhill,[1] R. S. Booth,[2]
S. P. Ellingsen,[3] J. R. Herrnstein,[1,4] D. L. Jauncey,[5] P. M. McCulloch,[3]
J. M. Moran,[1] R. P. Norris,[5] J. E. Reynolds,[5] A. K. Tzioumis,[5]

ABSTRACT

We present the first VLBI maps of H_2O maser emission (λ1.3 cm) in the nucleus of the Circinus Galaxy, constructed from data obtained with the Australia Telescope Long Baseline Array. The maser emission traces a warped, edge-on accretion disk between radii of 0.11 ± 0.02 and ~ 0.40 pc, as well as a wide-angle outflow that extends up to $\sim$ 1 pc from the estimated disk center. The disk rotation is close to Keplerian ($v \propto r^{-0.5}$), the maximum detected rotation speed is 260 km s^{-1}, and the inferred central mass is $1.7 \pm 0.3 \times 10^6$ M$_\odot$. The outflowing masers are irregularly distributed above and below the disk, with relative outflow velocities up to $\sim \pm 160$ km s^{-1}, projected along the line of sight. The flow probably originates closer than 0.1 pc to the central engine, possibly in an inward extension of the accretion disk, though there is only weak evidence of rotation in the outward moving material. We observe that the warp of the disk appears to collimate the outflow and to fix the extent of the ionization cone observed on larger angular scales. This study provides the first direct evidence (i.e., through imaging) of dusty, high-density, molecular material in a nuclear outflow < 1 pc from the central engine of a Seyfert galaxy, as well as the first graphic evidence that warped accretion disks can channel outflows and illumination patterns in AGN. We speculate that the same arrangement, which in some ways obviates the need for a geometrically thick, dusty torus, may apply to other type-2 AGN.

Subject headings: galaxies: active — galaxies: individual (Circinus galaxy) — galaxies: Seyfert — ISM: jets and outflows — ISM: molecules — masers

[1]Harvard-Smithsonian Center for Astrophysics, 60 Garden St, Cambridge, MA 02138 USA greenhill@cfa.harvard.edu, moran@cfa.harvard.edu

[2]Onsala Space Observatory, Chalmers Institute of Technology, Onsala, S-43992 Sweden roy@oso.chalmers.se

[3]University of Tasmania, School of Physics, GPO 252-21, Hobart, TAS 7001 Australia simon.ellingsen@utas.edu.au, peter.mcculloch@utas.edu.au

[4]Current address: Renaissance Technologies, 25 E. Loop Dr., Stony Brook, NY 11790 jrh@rentec.com

[5]Australia Telescope National Facility, P.O. Box 76, Epping, NSW 2121 Australia djauncey@atnf.csiro.au, rnorris@atnf.csiro.au, jreynold@atnf.csiro.au, atzioumi@atnf.csiro.au

1. Introduction

At a distance of 4.2 ± 0.8 Mpc (Freeman et al., 1977), the Circinus galaxy hosts one of the nearest Seyfert II nuclei. The bolometric luminosity is $\sim 4 \times 10^{43}$ ergs s^{-1}, $\sim 10\%$ of which is contributed by star formation in the inner ~ 100 pc (Moorwood et al., 1996). The central engine radiates 2×10^{42} erg s^{-1} (2-10 keV) and is obscured by a $n_H \sim 4 \times 10^{24}$ cm^{-2} column at energies lower than ~ 10 keV (Matt et al., 1999). Reflection by cool material dominates the X-ray spectrum, which includes a prominent (~ 2 keV equivalent width) Fe Kα fluorescence line (Matt et al., 1996). The optical spectrum includes coronal lines from photoionized gas (Oliva et al., 1994) and broad polarized Hα emission, which is ~ 3300 km s^{-1} wide and betrays the existence of an obscured broad line region (Oliva et al., 1998). The mass of the central engine has been uncertain. At 2.2μm wavelength, the central non-stellar source is < 1.5 pc in radius, and its dynamical mass is $< 4 \times 10^6$ M$_\odot$(Maiolino et al., 1998). Although massive, the central engine constitutes a small fraction of the nuclear mass, which including stars and gas amounts to $3.2 \pm 0.8 \times 10^8$ M$_\odot$ inside a radius of 140 pc (Curran et al., 1998).

The active galactic nucleus (AGN) of the Circinus galaxy drives a visible nuclear outflow on kpc scales, the position angle of which suggests an orientation for the central engine. Elmouttie et al., (1998) observe bipolar radio lobes, which lie at position angles (PA) of ~ 115 and $295^\circ \pm 5^\circ$. These are aligned with the minor axes of the galactic H I disk (PA= $300^\circ \pm 5^\circ$) (Freeman et al., 1977) and nuclear ^{12}CO ring (PA= $304^\circ \pm 4^\circ$), which lies between radii of 140 and 600 pc and is inclined by $78^\circ \pm 1^\circ$ (Curran et al., 1998). Circinus also exhibits a kpc-scale, one-sided optical ionization cone (Marconi et al., 1994) with an opening angle of $\sim 100^\circ$ and a mean PA$\sim 295^\circ$, approximately along the outflow axis. The ionization cone comprises knots and radial filaments whose kinematics are indicative of outward motion, possibly in the form of bullet-like ejecta, at speeds on the order of 100 to 200 km s^{-1} (Veilleux & Bland-Hawthorn 1997; Elmouttie et al., 1998; Wilson et al., 2000).

There is good evidence that extragalactic H_2O masers (λ1.3 cm) in NGC 4258, NGC 1068, and other galaxies (e.g., Miyoshi et al., 1995; Greenhill & Gwinn 1997) trace edge-on, warped accretion disks bound by central engines $\gtrsim 10^6$ M$_\odot$. Spectral-line interferometer data with milliarcsecond resolution straightforwardly provide accurate measurements of rotation curves, central engine masses, warp shapes, and disk orientations. The maser spectra in the systems that are the best examples exhibit complexes of "high-velocity" emission symmetrically bracketing "low-velocity" emission that is close to the systemic velocity of the host galaxy. In Circinus, H_2O maser emission has been known for over 20 years (Gardner & Whiteoak 1982), but only the relatively recent discoveries of spectral features blueward of the systemic velocity (Nakai et al., 1995; Braatz, Wilson, & Henkel 1996; Greenhill et al., 1997) have led to speculation that the masers in Circinus also trace an accretion disk.

We present the first maps of the Circinus H_2O maser source and report the detection of an accretion disk, bearing out the earlier speculation. We have also found that a fraction of the maser

emission originates outside the disk, in what appears to be a wide-angle outflow within ~ 1 pc of the central engine and aligned with the ionization cone. The discovery of this qualitatively new phenomenon introduces a fresh element to the study of AGN, because the locations and velocities of dense non-disk material in such close proximity to a central engine can be mapped for the first time. As a result, it is possible to test in new ways proposed mechanisms for the driving and collimation of outflows in AGN (e.g., Bottorff et al., 1997, and references therein).

In Sections 2, 3, and 4, we summarize our Very Long Baseline Interferometer (VLBI) observations, post-correlation analysis, and proposed model of a warped disk and outflow. In Section 5 we quantify the model and evaluate ramifications for collimation and driving mechanisms, and discuss the relation of the warped disk to the outflow and the ionization cone.

2. Observations

We observed the $6_{16} - 5_{23}$ transition of H_2O ($\nu_{\rm rest} = 22235.08$ MHz) toward Circinus three times in 1997 and 1998 (Table 1) with the Australia Telescope Long Baseline Array (LBA)[6], which provided baselines of ~ 200 to 1000 km. Table 2 summarizes the characteristics of the individual antennas. Typical tracks were 18 h at Mopra and Hobart, 12 h at Tidbinbilla, and 14 h at Parkes. Approximately every 1.5 h we observed a continuum source for ~ 0.5 h (PKS 0537-448, PKS 1424-418, PKS 1144-379, or PKS 1921-293) to enable calibration of the interferometer and antenna pointing at Parkes and Tidbinbilla.

We recorded two 16 MHz bandpasses (~ 215 km s^{-1}) at each station with an S2 VLBI terminal (Table 1). The S2 correlator at the Australia Telescope (AT) facility in Marsfield, NSW provided 1024 channels in each bandpass for cross-power and total-power spectra, following Fourier inversion of the correlation functions. The channel spacing was ~ 0.21 km s^{-1}, which provided at least three channels across the half-power full-width of the narrowest spectral components (e.g., see Nakai et al., 1995; Greenhill et al., 1997).

3. Calibration and Imaging

We calibrated the amplitudes, delays, and phases of the data with standard VLBI techniques, using the AIPS package of the NRAO[7] and the module ATLOD that is maintained separately by the AT.

---

[6]The Australia Telescope Long Baseline Array is part of the Australia Telescope, which is funded by the Commonwealth of Australia for operation as a National Facility managed by CSIRO.

[7]The National Radio Astronomy Observatory is operated by Associated Universities, Inc., under cooperative agreement with the National Science Foundation.

We computed a time-series of amplitude calibration factors for each station by fitting total-power spectra for the line triplet near 565 km s^{-1} (Figure 1) to template total-power spectra, constructed from data recorded at Mopra in 1997 July and Tidbinbilla in 1998 June. (We assume the radio astronomical definition of Doppler shift and heliocentric reference frame.) This calibration corrected for variations in antenna gain and atmospheric opacity. The template scans were calibrated with nominal system equivalent flux densities (SEFD) of 900 and 150 Jy, respectively, which provided a flux density scale accurate to $\sim 30\%$, given the elevations of the template scans and overall good weather conditions. The weak line strength and irregular spectral baselines at several stations in 1997 June precluded template fitting. Instead, amplitude calibrations were adjusted to maintain constant measured amplitude for the lines near ~ 565 km s^{-1} in the *cross-power* spectra, which is appropriate for relatively point-like emission. A total-power spectrum from Mopra, calibrated with the nominal SEFD, provided the absolute amplitude calibration.

We note that the quality of these amplitude calibrations was limited by the effects of interstellar scintillation, which in one instance has caused a doubling in line strength on time scales as short at 10 minutes (Greenhill et al., 1997). However, for the 1998 June and 1997 July epochs the effects of scintillation appear to have been relatively small. The total-power spectra constructed for the template fitting show variations in line strength of $\lesssim 30\%$ over time scales on the order of 30 minutes. Because we could not construct reliable templates for the 1997 June data, that epoch could have been more significantly affected by scintillation. This would reduce the dynamic range of images but not affect the centroid positions of individual emission features.

We used the calibrator scans to estimate delay, fringe rate, and fringe phase residuals induced by errors in the *a priori* station clocks and positions, and by electronics and the troposphere. We interpolated the delays and rates and applied them to scans of the maser. For the 1998 data, the calibration was accurate to ~ 2 ns and ~ 2 mHz in delay and rate, respectively. For the 1997 data, the accuracy for Mopra was worse, ~ 5 ns and ~ 5 mHz, because the maser clock was inadequately shielded against the (pointing-dependent) magnetic signature of the telescope structure. We also used observations of the calibrators PKS 1424-418 and PKS 1921-293 to estimate the time averaged (complex) bandpass response of each station. Overall, residual errors in calibration tended chiefly to scatter power in the synthesis images and reduce the dynamic range. Induced errors in the positions of emission features were ultimately much less than the size interferometer beam and did not affect the modeling.

The *a priori* position of the maser was another potential source of delay calibration error. Gardner & Whiteoak (1982) found that the emission lay within 10 to 15″ of the optical center for the nucleus (Freeman et al., 1977), which leaves a very large uncertainty. We analyzed the time variation of fringe rate for the 565 km s^{-1} line triplet observed in 1997 July to improve the astrometric position. A χ-squared minimization for a point-source model yielded a new position estimate, $\alpha_{2000} = 14^h13^m09\overset{s}{.}95 \pm 0^s.02$, $\delta_{2000} = -65°20'21\overset{''}{.}2 \pm 0\overset{''}{.}1$, where the quoted uncertainties include random and systematic components. This position is offset from the *a priori* position by $+1\overset{''}{.}5$ and $+0\overset{''}{.}1$ in right ascension and declination, respectively. We corrected the 1997 July data

and used the improved position estimate in correlation of the 1997 June and 1998 June epochs, after which the residual fringe rates were ~ 2 mHz (peak-to-peak) on even the longest baselines. This is consistent with the remaining $0\farcs1$ uncertainty.

To remove the effects of atmospheric path-length fluctuations at each epoch, we self-calibrated the emission within a few km s^{-1} of 565 km s^{-1} and applied the results to each spectral channel. We adjusted the weighting of data in the *(u,v)*-plane and the frequency-averaging of visibility data for each epoch, so that we could achieve a mean angular resolution of ~ 2.5 milliarcseconds (mas) and good signal-to-noise ratios (S/N). (We convolved the data with a 1.3 km s^{-1} wide boxcar, sampling every 0.65 km s^{-1} for 1997 June, a 0.87 km s^{-1} boxcar with sampling every 0.44 km s^{-1} for 1997 July, and a 0.44 km s^{-1} boxcar with sampling every 0.44 km s^{-1} for 1998 June.) The noise in the images (1σ) was 0.025 - 0.045 Jy, depending on the epoch and channel; the 1998 June observations were the most sensitive and best calibrated, with the broadest bandwidth (Table 1). To test the completeness of our census of emission detected in 1998 June, we also constructed images with natural weighting and achieved a sensitivity of 15 mJy over 0.44 km s^{-1}. In these images, we detected two new emission clumps at the red and blue extrema of the measured spectrum. In the end, we detected emission between 179 and 699 km s^{-1}(Figure 1).

The synthesized beamwidths were 3.7×2.0 mas at PA $= 77^\circ$ (1997 June), 3.7×1.4 mas at PA $= 80^\circ$ (1997 July), 3.6×1.9 at PA$= 84^\circ$ (1998 June 27), and 4.0×1.4 mas at PA$=-79^\circ$ (1998 June 28). We fit a 2-D Gaussian model brightness distribution to each emission "maser spot" stronger than 5σ in each deconvolved image. Because the image pixels are partially correlated, we adopted a position uncertainty for each fitted Gaussian that was (1) the formal fitting error or (2) the statistical error dictated by the beamwidth divided by $2 \times S/N$ (Reid & Moran 1988; Fomalont 1999), whichever was larger. To this uncertainty, we added in quadrature a term accounting for the effect of possible error in the absolute position of the 565 km s^{-1} emission ($0\farcs1$). This term contributed 35μas per 100 km s^{-1} of velocity offset from 565 km s^{-1}. For 1998 June and 1997 July, the spreads in spot positions for individual clumps of emission are consistent with the computed total position uncertainties. The larger spreads observed in 1997 June are suggestive of an unmodeled systematic component of position uncertainty, probably stemming from the lower quality calibration and limited coverage of the *(u,v)*-plane for that epoch.

4. Results and Interpretation

At each epoch, the sky distribution of maser emission appears to comprise two populations (Figure 2) that we will argue sample a roughly edge-on warped accretion disk as well as an outflow of material from the vicinity of the central engine. There is a thin, densely sampled, S-shaped locus that comprises redshifted emission to the west, and blueshifted emission to the east. The arms of the S exhibit velocity gradients along their lengths with increasingly large Doppler shifts (relative to the systemic velocity) toward the center. Most of the remainder of the maser emission comprises knots that lie outside the S and away from the putative disk. However, even when relatively close

to the S, the line-of-sight velocity of the non-disk maser emission is offset by tens of km s^{-1}. We propose that this non-disk emission originates in a wide-angle nuclear outflow.

The velocities of the most red and blueshifted maser spots, 179 km s^{-1} and 699 km s^{-1} (Figure 1), symmetrically bracket the nominal systemic velocity of Circinus, 439 ± 2 km s^{-1}(Freeman et al., 1977; Curran et al., 1998). The overall spectrum and sky distribution changed from epoch to epoch, with emission features coming and going, probably because of natural variation in the intensities of individual emission features, as well as interstellar scintillation. To obtain the most complete assessment of the extent of dense molecular structure that underlies the maser emission in Circinus, we superposed the maps for two well separated epochs, 1997 July and 1998 June (Figure 3). To register the two maps, we aligned the positions of the common emission peak at 565.2 km s^{-1}. A comparison of relative positions for other features that are present in both maps suggests the registration uncertainty is $\lesssim 0.15$ mas.

5. Discussion

5.1. The warped disk

We interpret the distribution of maser emission in Circinus in the context of the warped accretion disk in NGC 4258, which has been well modeled (e.g., Herrnstein, Greenhill, & Moran 1996). In general, maser emission in warped disks is beamed toward the observer from regions where the gradient in line-of-sight velocity along the line of sight is close to zero and the disk is approximately tangent to the line of sight. This corresponds to two loci, the "midline," where the orbital velocity is parallel to the line of sight, and an arc along the near side of the disk, where the orbital velocity is nearly perpendicular to the line of sight. The former is responsible for high-velocity emission that traces the rotation curve of the disk, and the latter is associated with low-velocity emission. The detailed spatial and velocity distribution of observable high- and low-velocity emission is also affected by the geometry of the warp, which (1) determines the solid angle into which emission is beamed, (2) shadows parts of the disk from X-ray emission by the central engine, which otherwise heats gas and probably supports maser emission (Neufeld, Maloney, & Conger 1994; Neufeld & Maloney 1995; Collison & Watson 1995; Wallin & Watson 1997), and (3) determines how the disk might overlie and thereby amplify background nonthermal continuum emission, such as from a jet (e.g., Herrnstein et al., 1997).

A warped disk model for Circinus (see Table 3) receives its strongest support from the following: (1) the elongated, antisymmetric angular distribution of maser spots that forms the shallow S in Figure 3, (2) the symmetric bracketing of the nominal systemic velocity by the most highly red and blueshifted emission, (3) the antisymmetric distribution of Doppler shifts along the S with velocity declining by roughly $b^{-0.5}$, where b is impact parameter (Figure 4), and (4) the orientation of the inner disk (as seen in projection), more or less perpendicular to the axis of the known radio lobes (Elmouttie et al., 1998) and ionization cone (Marconi et al., 1994; Veilleux & Bland-Hawthorn

1997; Wilson et al., 2000).

To establish which maser spots arise in the disk, we fit a second order polynomial to the sky position of the midline, which is identifiable because that is where the greatest Doppler shifts are observed (Figure 3), and we calculated the angular offset between each maser spot and the midline. We classified emission that is offset by < 1 mas (about one half beamwidth, north-south, in 1998 June) as disk emission (Figure 5). About 43% of the integrated emission we detected in 1998 June arises in the disk, and on average, maser spots in and out of the disk are comparably bright. The non-disk emission alone occupies the center ~ 260 km s^{-1} of the spectrum, while the disk emission lies on either side in velocity (Figure 6). There is some overlap in velocity, the extent of which depends on the chosen cutoff to the angular offset from the midline (i.e., here, 1 mas). This overlap may be a consequence of resolved disk thickness, azimuthal structure and a not quite edge-on orientation, or interaction between the disk and the outflow whereby the fastest spots (in projection) within the outflow lie closest to the disk.

The position of the dynamical center of the disk, its inner (observed) radius, and peak rotation speed may be estimated from the innermost red and blueshifted masers, for which we assume a common edge-on orbit. The peak observed rotation speed, V_{max}, is 260 km s^{-1} in an orbit at a position angle of 29° with radius, $r_{\rm in}$, of 5.3 ± 0.1 mas (0.11 ± 0.02 pc, including the uncertainty in distance). The inferred disk center lies at 17.6 and 13.1 mas east and north of the origin in the maps in Figures 2 and 3. Taking into account only gravity and assuming circular motion, we infer an enclosed mass, $M(r < r_{in})$, of $1.7 \pm 0.3 \times 10^6$ M$_\odot$ or mean mass density of $3.2 \pm 0.9 \times 10^8$ M$_\odot$ pc^{-3}. We note that because the disk does not display identifiable low-velocity emission on the near side, it is difficult to estimate inclination directly (cf. NGC 4258; Miyoshi et al., 1995). Formally, the mass and density estimates depend on the inclination and are lower limits. However, we argue that the disk must be close to edge-on because the masers cluster tightly around a sharply defined disk midline.

The orientation of the innermost orbit on the disk is close to perpendicular to the flow axes of the known bipolar radio lobes (Elmouttie et al., 1998) and wide-angle CO outflow cone (Curran et al., 1999), the rotation axes of the H I galactic disk (Freeman et al., 1977) and the circumnuclear CO disk of radius 140 to 600 pc (Curran et al., 1998), and the principle axis of the most prominent [O III] filament in the ionization cone, for which the position angle is $\sim -50°$ (Veilleux & Bland-Hawthorn 1997). However, the assumed 90° inclination of the disk at the inner radius is somewhat offset from the $65° \pm 2°$ inclination of the galactic disk (Freeman et al., 1977), the $78° \pm 1°$ inclination of the CO disk (Curran et al., 1998), and the $\sim 65°$ inclination inferred by Wilson et al., (2000) for a 40 pc-radius ring of H II regions centered on the central engine. Some of these alignments are sensible, such as the position angles of the inner accretion disk and the radio lobe axis. However, others may include an element of coincidence, such as the alignment between the circumnuclear CO disk and the accretion disk, for which agreement with the inner orbital axis is better than agreement with the outer orbital axis (Table 3). Overall, we suggest that the orientation of the accretion disk should be only weakly coupled via gravity to the surrounding large-scale dynamical

structures, because the central engine contributes only $\sim 0.5\%$ of the 3.2×10^8 $M_\odot$ inside 140 pc and has a sphere of influence less than a few parsecs in radius (Curran et al., 1998).

The inferred peak rotation velocity as a function of impact parameter, b, measured from the estimated dynamical center, declines approximately as $b^{-0.5}$ (Figure 4), which is suggestive of a relatively low-mass disk, as is observed in NGC 4258 (Miyoshi et al., 1995). However, a disk that is both massive and warped in inclination angle could have a similarly steep rotation curve. Specifically, if a disk is edge-on at radius $r_\circ$ but inclined by δi at a radius $r + \delta r$, then it will display the same apparent rotation speed as a flat, edge-on, Keplerian disk if the fractional disk mass $M_{\rm disk}/M$ is $\tan^2(\delta i)$, where M is the encircled mass at radius $r_\circ$. In order to place a limit on the disk mass for Circinus, we assume that the disk is warped both in position and inclination angles, and that the warps are of the same order of magnitude, $\sim 27^\circ$ between 0.11 and 0.40 pc (see Table 3). Hence, our data are consistent with a fractional mass of 26%, or $\sim 4 \times 10^5$ $M_\odot$. In the absence of an actual measurement of the inclination warp, we adopt this mass estimate as an upper limit.

The relatively high particle densities inferred from the presence of H_2O maser emission — 10^8 to 10^{10} cm^{-3} for a H_2O fractional abundance of 10^{-5} to 10^{-4} (Elitzur 1992) — are also consistent with a relatively massive disk. For a uniform particle density and a planar disk, the disk mass enclosed inside radius r is $\sim 1.4 \times 10^6 n_{10} \gamma r_{-1}^3$ $M_\odot$, where r_{-1} is the radius in units of 0.1 pc, n_{10} is density in units of 10^{10} cm^{-3}, and γ is the height of the disk as a fraction of its radius. Hydrostatic equilibrium dictates a lower limit on γ that is on the order of $c_s/v_{\rm rot}$, where c_s is the sound speed (~ 1.6 km s^{-1} for gas at 400 K). Our upper limit on disk mass inside 0.40 pc ($\sim 4 \times 10^5$ $M_\odot$), is consistent with a 4×10^9 cm^{-3} upper limit on density, for $v_{\rm rot} \sim 140$ km s^{-1} and hydrostatic equilibrium, which agrees with expectations.

Estimates of the Toomre Q-parameter for gas densities sufficiently high to support maser action ($> 10^8$ cm^{-3}) indicate that self-gravity is important and probably causes clumping of disk material. We note that the distributions of disk masers on the sky (Figure 3) and in the position-velocity diagram (Figure 4) exhibit substantial substructure, which may be a signature of clumping. This clumping could limit the maser gain paths in the disk and thus be responsible for the comparable strengths of the disk and non-disk emission. The Toomre Q-parameter is $c_s \Omega / \pi G \Sigma$, where Ω is the angular rotation speed, and Σ is the mass surface density. Instabilities arise for $Q < 1$. By assuming the disk thickness is η times the hydrostatic limit, we obtain $Q \sim 0.6 M_6 / \eta n_{10} r_{-1}^3$, where M_6 is the central engine mass in units of 10^6 $M_\odot$. For $n = 4 \times 10^9$ cm^{-3}, $r = 0.40$ pc, and hydrostatic equilibrium ($\eta = 1$), $Q \sim 0.04$. The Q-parameter could be even smaller if the apparent thickness of the disk (which is on the order of a few tenths of a mas) is real and thereby much greater than the hydrostatic limit (which is about tens times smaller). However, it is difficult to distinguish between measurable disk thickness and nonaxisymmetric structure (e.g., Maoz & McKee 1998), because the disk is highly inclined and the angular resolution of our observations is an order of magnitude larger than the putative thickness.

5.2. The clumpy wide-angle outflow

The association of water maser emission with a bipolar wide-angle wind in an AGN is qualitatively new and distinct from the reported connection to jet activity in some galaxies [i.e., NGC 1068 (Gallimore et al., 1996), NGC 1052 (Claussen et al., 1998), NGC 3079 (Trotter et al., 1998), and Mrk 348 (Peck et al., 2001)]. Less than 1 pc from a central engine, outflowing material is often assumed to be photoionized, but away from the flow axis, gas columns may be large enough ($10^{22\pm1}$ cm^{-2}) to maintain a molecular component with internal pressures (p/k) that are $\sim 10^{11}$ to 10^{13} K cm^{-3} (Emmering, Blandford, & Shlosman 1992; Königl & Kartje 1994; Kartje, Königl, & Elitzur 1999). Maser emission can be readily stimulated in this gas by X-ray heating (Neufeld, Maloney, & Conger 1994; Neufeld & Maloney 1995) or shock heating (Elitzur, Hollenbach, & McKee 1989; Kaufman & Neufeld 1996), if turbulence and gradients in line-of-sight velocity permit.

In Circinus, blueshifted "outflow masers" lie south and east of the central engine, and redshifted counterparts lie chiefly to the west (Figures 2, 3, & 5). The line-of-sight velocities of these masers are offset from the systemic velocity by up to $\sim \pm 160$ km s^{-1} (Figure 6), though we note a few maser spots that are somewhat more redshifted and that lie almost due west of the dynamical center in 1997 July. To start, we infer that this emission originates outside the disk because (1) it lies up to ~ 1 pc from the disk center, while the disk midline can be traced only between radii of 0.11 to ~ 0.40 pc, (2) many of the non-disk masers lie close to the disk rotation axis, as seen in projection, (3) the line-of-sight velocities of the non-disk masers that instead lie close to the disk differ by tens of km s^{-1} from the velocities of adjacent disk material, and (4) the non-disk masers display no systematic gradient in line-of-sight velocity as a function of position angle relative to the disk center (Figure 7), as would be expected were they to lie in a disk sufficiently warped to include them. Having excluded a disk origin, we infer that the masers in question are associated with outflow because it is unlikely that material close to the axis of an accretion disk, and also within 1 pc of a supermassive blackhole would be infalling. (We note that it is also unlikely that the non-disk masers are associated with a relaxed central cluster of mass losing stars, principally because the distribution of masers is not at all centered on the inferred position of the central engine.)

We adopt a bipolar, cone-like model geometry to describe the outflow (Figure 8). Emission with different Doppler shifts is well mixed on the sky (e.g., Figure 7). This is suggestive of relatively short gain paths peppering the outflow volume, where emitting regions that move along very different trajectories lie along proximate lines of sight (i.e., the masers probably do not just lie along the limbs of the outflow). Within this volume, the masers presumably do lie toward the front because of the opacity of the photoionized gas that probably lies between the maser-emitting regions (see below).

Although a compelling general case may be made for outflow, we cannot explain the observed angular distributions and Doppler shifts of the outflow masers in detail. The chief hurdles are (1) the prevalence of blueshifted emission to the south and east of the disk center and redshifted

emission on the reverse side, and (2) the difference in angular distributions on opposite sides of the accretion disk, where some areas are devoid of visible maser emission while their counterparts (mirrored on the other side of the disk) are not (Figure 3). The blue-red asymmetry in the outflow could indicate that the flow is inclined to the line of sight, despite the putative edge-on orientation of the accretion disk. However, it is difficult to test this hypothesis because the redshifted outflow is poorly sampled on the sky and almost entirely defined by maser emission at low latitudes (i.e., in close proximity to the disk). Gas dynamic or magnetic coupling between outflowing and rotating disk material could be responsible for the observed Doppler shifts at low latitudes, and in position-velocity space, for some portion of the structure we observe near (the representation of) the disk midline (see Figure 4). Regarding the second hurdle, the difference in maser distribution above and below the disk could be a consequence of differential extinction. However, if the axis of the outflow is close to the plane of the sky, then this effect would be small. Alternatively, the angular distributions could depend chiefly on where velocity coherent maser gain paths happen to exist. In general, the longest paths are probably associated with limb-brightening and motions that are closer to the plane of the sky than to the line of sight (e.g., Elitzur, Hollenbach, & McKee 1992). This observation may answer the question, why do we not see highly blueshifted outflow material close to the line of sight toward the central engine. However, it is not clear whether it can explain the absence of a broad distribution on the sky of redshifted outflow masers.

Because water masers require high gas densities, their presence broadly distributed in the outflow argues that it must be inhomogenous or "clumpy." Were the outflow smooth, the associated mass loss would be prohibitively large, $\sim 6 \times 10^3 r_{-1}^2 n_{10} v_2$ $M_\odot$ yr^{-1}, where v_2 is velocity in units of 100 km s^{-1}. For a 100 km s^{-1} flow that is 10^9 cm^{-3} at a radius of 0.1 pc, the flow would consume a mass equivalent to the central engine and accretion disk in only a few $\times 10^3$ years. However, the appearance of the flow, as traced by maser emission, is at best sparse and irregular. If this is representative and not merely a consequence of anisotropic beaming of maser radiation, then the mass loss would be orders of magnitude smaller. For instance, if the rate of loss balances the rate of accretion, then the mean density of the outflow at 0.1 pc radius is $\sim 10^4$ cm^{-3}, where we express the accretion rate as $1.7 \times 10^{-4} L_{43} \epsilon^{-1}$, and where L_{43} is the bolometric luminosity in units of 10^{43} ergs s^{-1} and ϵ is the accretion efficiency of the central engine, probably ~ 0.1. The apparent mean clump-interclump density contrast is on the order of 10^5, and the shielding column in the interclump medium is on the order of 10^{22} cm^{-2} for a path length comparable to the disk radius, as required (Kartje, Königl, & Elitzur 1999). (We note that the flow could instead contain pockets of molecular gas with a range of sizes and densities that span orders of magnitude, only some of which would be conducive to observable maser action. This would affect the estimates of density contrast and shielding column, but it would not reduce the imperative that the flow be inhomogeneous.)

5.3. Collimation by the warped disk

The angular distribution of the outflow masers is consistent with the hypothesis that excitation depends on a direct line of sight to the central engine. In the shadow of the disk (i.e., in regions where this path is blocked) no maser emission was detected (Figure 8). We suggest that this shadowing is a physical blockage of both radiation and mechanical energy through which *the warped accretion disk collimates the nuclear outflow.* Channeling on such small scales is consistent with the inference by Wilson et al., (2000) based on HST imaging, that the Circinus ionization cone is collimated within 2 pc of the central engine. In the proposed model, on each side of the maser disk, one radial edge of the outflow is determined by the position angle of the disk at the inner radius, and the other edge is fixed by the concave surface of the disk warp along which the outflow brushes, up to the outer radius of the disk.

We estimate the outer radius to be ~ 0.40 pc based on the close packing of disk masers along the midline up to this radius, the angular distribution of outflow masers at larger radii, and the extent of the ionization cone. First, the midline of the warped disk is traced in the maps (Figure 3) and the position-velocity diagram (Figure 4) by a relatively continuous locus of maser spots up to a radius of ~ 0.40 pc. Beyond 0.40 pc, an extrapolation of the midline does pass close to some other masers, but they do not lie on the Keplerian rotation curve. Second, the only way in which the southwesternmost maser clump near position (-16, -8) mas in Figure 3 can achieve a direct line of sight to the central engine is if the disk is truncated at ~ 0.40 pc. Third, the southern edge of the ionization cone, observed in [O III] light (Marconi et al., 1994; Veilleux & Bland-Hawthorn 1997; Wilson et al., 2000), lies at a position angle of $\sim -120°$, which is close to the position angle of the disk midline at a radius of ~ 0.40 pc. Were the warped disk to extend substantially beyond this proposed outer radius, the disk would block a larger solid angle of radiation and create a different southern limit for the ionization cone. We speculate that an outer radius of ~ 0.40 pc may also be associated with the presence of a maser spot cluster surrounding the outer tip of the redshifted midline, forming a backward "C" visible near the origin in Figures 3 and 5. These masers move with sub-Keplerian velocities and could correspond to material lost from the outer disk where it is roughened by interaction with outflow and radiation.

The putative outer radius of the accretion disk constrains the longevity of activity in Circinus at the observed luminosity, 4×10^{43} ergs s^{-1}. The wide-angle outflow restricts the solid angle (as seen from the central engine) over which material can fall in and replenish the accretion disk. The outflow blocks 80% to 90% of the surroundings. If the supply of new material is thereby reduced, then for the accretion rate ($1.7 \times 10^{-4} L_{43} \epsilon^{-1}$) that corresponds to an efficiency of 10%, the accretion disk will be exhausted in ~ 6 Myr for the previously estimated maximum disk mass of 4×10^5 M$_\odot$.

5.4. The Origin of the Outflow

Two possible origins for the molecular outflow are: (1) radial ejection of ionized broad line clouds that form dust and molecules as they cool, and (2) uplift and ejection of warm molecular disk material. The association of masers and cooled broad line cloud material is largely circumstantial. It rests on the observation that the densities and temperatures required for maser emission are consistent with adiabatic expansion of material with intial densities and temperatures on the order of 10^{11} cm^{-3} and 10^4 K (e.g., Kaspi & Netzer 1999; Korista & Goad 2001, and references therein), assuming an adiabatic constant of $\sim \frac{5}{3}$. However, it is not clear whether maser action is possible in freely expanding clouds, where velocity gradients and turbulent motions may be significant, or in the shocks that may arise within or ahead of the clouds. The observed line-of-sight outflow velocities, which are smaller than the Keplerian rotation velocity and thereby the escape velocity at all radii, are a secondary concern. Because the motions of the observable masers may lie somewhat preferentially toward the plane of the sky (see Section 5.2), the too small velocities may be a projection effect.

In order to describe self-consistently the geometry and dynamics of broad line regions, Emmering, Blandford, & Shlosman (1992) modeled a hydromagnetic wind created by the uplift and ionization of clumps from a cool molecular accretion disk. The magnetic field, anchored in the disk, confined the ionized clouds and imparted rotation to the outflow. Over time, the clouds moved outwards with increasingly radial trajectories as the azimuthal field component or cloud coupling to the field weakened (see, e.g., Bottorff et al., 1997). Königl & Kartje (1994) expanded this model by showing that the hydromagnetic disk wind could be clumpy, dusty, and molecular over a broad range of latitudes. They suggested that such a wind might be responsible in general for the obscuration observed toward type-2 AGN, rather than oft posited geometrically thick tori. Kartje, Königl, & Elitzur (1999) applied the model to the stimulation of maser emission in the uplifted clumps once they rise from the disk to be irradiated by the central engine. (We note that in this picture, the disk is not directly the source of maser radiation.)

The hydromagnetic wind model is somewhat more attractive than the simple ejection model for broad line clouds principally because in the former the clumps are magnetically confined. They do not need to expand by orders of magnitude and remain coherent to achieve temperatures and densities conducive to maser action. However, we note that in the limit where outflowing material moves largely radially well after uplift, the models are similar. The simple ejection model as stated finesses the origin of the broad line clouds, but if the clouds originate in an accretion disk, then the models differ chiefly in whether the disk material remains neutral after it is removed from the disk.

However, the hydromagnetic wind model, as applied by Kartje, Königl, & Elitzur (1999) makes three predictions that are not easily reconciled with the observations. First, the masers should lie away from the rotation axis of the disk. In contrast, we observe outflow masers that are apparently quite close to the rotation axis. If this material is removed from the observed accretion disk (between radii of ~ 0.1 and ~ 0.4 pc), then it would have to travel almost vertically as it is

uplifted. Second, masers in a hydromagnetic wind should exhibit a sub-Keplerian rotation curve (i.e., in a position-velocity diagram the masers would at least in part lie above the disk rotation curve). In fact, the signature of rotation is weak if present at all, and for any given radius, the Doppler shifts of outflow material are smaller than for the disk. Third, the wind should support maser emission close to the loci where dust sublimation occurs, resulting in a more or less flattened X-pattern on the sky for relatively edge-on orientations. However, the actual distribution of masers is dichotomous, featuring a sharply defined, thin, S-shaped disk *and* a broad outflow component.

We propose a modified wind model. First, the outflow begins well inside the observed inner radius of the disk and thereby can reach high latitudes at radii of 0.1 to 0.4 pc more readily. Very high velocity maser emission, offset up to ~ 400 km s^{-1} from the systemic velocity, has recently been discovered in Circinus (Greenhill et al., 2003). If the emission originates in the accretion disk, it provides evidence for a resevoir of molecular material ~ 0.03 pc from the central engine. Second, the uplifted material moves by and large radially, perhaps because it decouples quickly from the magnetic field threading the accretion disk. Third, the outflow is sparsely populated with clumps of material, so that the warped accretion disk at larger radii is not significantly shadowed and can emit maser radiation, as is observed.

6. Conclusions and Comment

We find that the H_2O maser emission in the Circinus Galaxy traces a warped, edge-on accretion disk at radii between 0.11 ± 0.02 pc and ~ 0.40 pc. The peak observed disk rotation velocity is ~ 260 km s^{-1}, and the encircled mass is $1.7 \pm 0.3 \times 10^6$ M$_\odot$. The implied ratio of bolometric luminosity to Eddington luminosity is ~ 0.2. The rotation curve is nearly Keplerian and the disk mass is probably $< 24\%$ of the central mass. Given the (low) rotation speed of the disk, this is substantial enough to cause clumping due to self-gravity, which may explain observed substructure in the disk. The inner radius of the maser disk is comparable to the well resolved maser disk in NGC 4258 (0.14 pc), even though the X-ray luminosity of Circinus is ~ 10 times larger (Makishima et al., 1994; Reynolds et al., 2000). If the recently reported very high velocity emission in Circinus originates in the disk (Greenhill et al., 2003), then the paradox is more striking still. However, it is possible the inner radii of maser emission are not dictated by dust sublimation. The discrepancy may be due to the geometries of the warped disks. For example, in NGC 4258 maser emission at particularly small radii may not be directed toward us.

A second population of masers in the Circinus AGN traces a wide-angle outflow up to ~ 1 pc from the central engine with line-of-sight velocities of up to $\sim \pm 160$ km s^{-1} with respect to the systemic velocity. These masers are the first direct evidence (i.e., provided by imaging) of dusty, high-density, molecular material in a nuclear outflow, at such small scales. The mechanism that drives the wind is uncertain but may be hydromagnetic. The wind is observed in the regions around the disk that are not shadowed by the warp, from which we suggest that the disk channels the outflow and occults radiation from the central engine. The position angles of the edges of the

outflow correspond well to those of the outflow and ionization cone observed on scales of hundreds of parsecs (Veilleux & Bland-Hawthorn 1997; Curran et al., 1999). Here too, Circinus may provide the first direct evidence for collimation of an AGN outflow and illumination pattern by a warped accretion disk. In the classical paradigm for AGN, a geometrically thick tori has been cast in this role, even though it has been difficult to explain how such structures can be supported vertically (e.g., Krolik & Begelman 1988). For Circinus and perhaps other type-2 AGN, sub-parsec, warped accretion disks are a simpler explanation of a breadth of observations.

It is an open question whether thick tori are required at all to explain the X-ray obscuring columns observed in type-2 AGN. Warped disks of the type found in NGC 4258 and Circinus could easily supply the needed column densities, but they are relatively flat. These two disks subtend on the order of 10 to 20% of the sky as seen from their respective central engines and do not readily explain the high proportion of obscured AGN out of the total (e.g., Miller & Goodrich 1990). As suggested by Königl & Kartje (1994), dusty hydromagnetic winds may be a general source of obscuration. Alternatively, structures on the small spatial scales of broad line regions (Risaliti et al., 2002) or the > 100 pc scales of warped CO gas disks (Schinnerer et al., 2000) and other dusty galactic structures (Malkan et al., 1998) may be important.

The Circinus H_2O maser is the third one for which detailed VLBI study has detected disk structure and a declining rotation curve. As has been demonstrated for the NGC 4258 and NGC 1068 masers, the Circinus maser makes possible unusually detailed study of the structure and dynamics of a region < 1 pc from what is most probably a supermassive black hole. We anticipate that higher angular resolution VLBI observations covering the recently recognized, full ~ 900 km s^{-1} breadth of the maser will improve our understanding of the structure of the ~ 0.1 pc radius warped accretion disk and the mechanism that drives the wide-angle outflow apparently emanating from still closer to the black hole.

We thank W. Wilson and R. Ferris for their support of the S2 VLBI correlator, and H. May and S. Amy for network and software support. We acknowledge the helpful comments of G. Ball, M. Elitzur, A. Konigl, and an anonymous referee. We are grateful for the dedication of the staff at the LBA antennas. We acknowledge the use of the NASA/IPAC Extragalactic Database (NED), which is operated by the Jet Propulsion Laboratory, California Institute of Technology, under contract with the National Aeronautics and Space Administration.

REFERENCES

Bottorff, M., Korista, K. T., Shlosman, I., & Blandford, R. D. 1997, ApJ, 479, 200

Braatz, J. A., Wilson, A. C. S., & Henkel, C. 1996, ApJS, 106, 51

Claussen, M. J., Diamond, P. J., Braatz, J. A., Wilson, A. S., & Henkel, C. 1998, ApJ, 500, L129

Collison, Alan J., & Watson, William D. 1995, ApJ, 452, L103

Curran, S. J., Johansson, L. E. B., Rydbeck, G., & Booth, R. S. 1998, A&A, 338, 863

Curran, S. J., Rydbeck, G., Johansson, L. E. B., & Booth, R. S. 1999, A&A, 344, 767

Elitzur, M., Hollenbach, D. J., & McKee, C. F. 1989, ApJ, 346, 983

Elitzur, M., Hollenbach, D. J., & McKee, C. F. 1992, ApJ, 394, 221

Elitzur, M. 1992, "Astronomical Masers," (Dordrecht: Kluwer)

Elmouttie, M., Haynes, R. F., Jones, K. L., Sadler, E. M., & Ehle, M. 1998, MNRAS, 297, 1202

Emmering, R. T., Blandford, R. D., & Shlosman, I. 1992, ApJ, 385, 460

Fomalont, E. B. 1999, in Synthesis Imaging in Radio Astronomy II, eds. G. B. Taylor, C. L. Carilli, & R. A. Perley, (San Francisco: ASP), 307

Freeman, K. C., Karlsson, B., Lynga, G., Burrell, J. F., van Woerden, H., Goss, W. M., & Mebold, U. 1977, A&A,.55, 445

Gallimore, J. F., Baum, S. A., O'Dea, C. P., Brinks, E., & Pedlar, A. 1996, ApJ, 462, 740

Gardner, F. F., & Whiteoak, J. B 1982, MNRAS, 201, P13

Greenhill, L. J., Ellingsen, S. P., Norris, R. P., Gough, R. G., Sinclair, M. W., Moran, J. M., & Mushotzky, R. 1997, ApJ, 474, L103

Greenhill, L. J., & Gwinn, C. R. 1997, Ap&SS, 248, 261

Greenhill, L. J., Kondratko, P. T., Lovell, J. E. J., Kuiper, T. B. H., Moran, J. M., & Jauncey, D. L. 2003, ApJL, 582, L11

Herrnstein, J. R., Greenhill, L. J., & Moran, J. M. 1996, ApJL, 468, L17

Herrnstein, J. R., Moran, J. M., Greenhill, L. J., Diamond, P. J., Miyoshi, M., Nakai, N., & Inoue, M. 1997, ApJL, 475, 17

Kartje, J. F., Knigl, A., & Elitzur, M. 1999, ApJ, 513, 180

Kaspi, S., & Netzer, H. 1999, ApJ, 524, 71

Table 1. Journal of Long Baseline Array Observations

Date	Array[1]	Bandpasses[2]		Notes
		(km s^{-1})	(km s^{-1})	
1997 June 24	Pk-Mo-Ho-Td	233–449	454–670	No fringes at Td for 80% of track.
1997 July 25	Mo-Ho-Td	234–450	455–671	No fringes at Pk.
1998 June 27	Pk-Mo-Ho-Td	313–529	488–704	···
1998 June 28	Pk-Mo-Ho-Td	151–367	488–704	···

[1]Pk–Parkes, NSW (Parkes); Td–Canberra, ACT (Tidbinbilla); Mo–Coonabarabran, NSW (Mopra); Ho–Mt. Pleasant, Tasmania (Hobart).

[2]Heliocentric velocities with respect to the radio definition of Doppler shift. Optical velocities are up to 1.6 km s^{-1} larger over the range of velocities observed.

Table 2. The LBA at λ1.3cm (c. 1997/1998)

Telescope	Mount	Diameter (m)	SEFD[1] (Jy)	Receiver
Parkes	Alt-Az	64	700	cooled HEMT; prime focus
Mopra	Alt-Az	22	900	cooled HEMT; cassegrain focus
Hobart	X-Y[2]	26	5000	uncooled HEMT; prime focus
Tidbinbilla	Alt-Az	70	150	cooled HEMT; cassegrain focus

[1]Nominal values under good weather conditions and moderate elevation. Calibration of values for each observation and the elevation dependence is discussed in section §3.

[2]X–Y mount with a north-south axis of motion.

Table 3: The Warped Accretion Disk and Central Engine

Reference[1] α_{2000}	$14^h13^m09\overset{s}{.}95 \pm 0\overset{s}{.}02$
δ_{2000}	$-65°20'21\overset{''}{.}2 \pm 0\overset{''}{.}1$
$r_{\rm inner}$	0.11 ± 0.02pc [2]
$r_{\rm outer}$	~ 0.40 pc [2]
$V_{\rm orbital}(r = r_{\rm inner})$	260 km s^{-1} [4]
$M(r < r_{\rm inner})$	$1.7 \pm 0.3 \times 10^6$ M$_\odot$
$\rho(r < r_{\rm inner})$	$3.2 \pm 0.9 \times 10^8$ M$_\odot$ pc^{-3}
Period $(r = r_{\rm inner})$	2600 ± 500 yr
α $(V \propto r^\alpha)$	~ -0.5
$PA(r = r_{\rm inner})$	$29° \pm 3°$
$PA(r = r_{\rm outer})$	$56° \pm 6°$
$M_{\rm disk}(r_{\rm inner} < r < r_{\rm outer})$	$< 4 \times 10^5$ M$_\odot$ [5]

[1] Position of the maser emission at 565.2 km s^{-1} in 1997 July. The center of the disk (i.e., the central engine) was offset 17.6 mas east and 13.1 mas north. The optical nucleus is offset by $-1\overset{''}{.}5$ and $-0\overset{''}{.}1$ in right ascension and declination, respectively (Freeman et al., 1977).

[2] For an assumed distance of 4.2 Mpc (Freeman et al., 1977).

[3] Adopted from Freeman et al., (1977); Curran et al., (1998).

[4] Assuming the disk is edge-on at the inner radius.

[5] Computed on the premise that the moderating effect of a substantive disk mass on the slope of the rotation curve is balanced by the steepening effect of a warp in inclination, leaving a Keplerian rotation curve. The largest probable change in inclination (from 90° at $r_{\rm inner}$) is on the order of the observed change in position angle, $\sim 27°$. See Section 5.1.

Kaufman, M. J., & Neufeld, D. A. 1996, ApJ, 456, 250

Königl, A., & Kartje, J. F. 1994, ApJ, 434, 446

Korista, K. T., & Goad, M. R. 2000, ApJ, 536, 284

Krolik, J. H., & Begelman, M. C. 1988, ApJ, 329, 702

Maiolino, R., Krabbe, A., Thatte, N., & Genzel, R. 1998, ApJ, 493, 650

Makishima, K., et al., 1994, PASJ, 46, 77

Malkan, M. A., Gorjian, V., & Tam, R. 1998, ApJS, 117, 25

Maoz, E., & McKee, C. F. 1998, ApJ, 494, 218

Marconi, A.,Moorwood, A. F. M., Origlia, L., & Oliva, E. 1994, Messenger, 78, 20

Matt, G., Fiore, F., Perola, G. C., Piro, L., Fink, H. H., Grandi, P., Matsuoka, M., Oliva, E., & Salvati, M. 1996, MNRAS, 281, L69

Matt, G., et al., 1999, A&A, 341, L39

Miller, J., S., & Goodrich, R. W. 1990, ApJ, 355, 456

Miyoshi, M., Moran, J., Herrnstein, J., Greenhill, L., Nakai, N., Diamond, P., & Inoue, M. 1995 Nature, 373, 127

Moorwood, A. F. M. et al., 1996, A&A, 315, L109

Nakai, N., Inoue, M., Miyazawa, K., Miyoski, M., & Hall, P. 1995, PASJ, 47, 771

Neufeld, D. A, Maloney, P. R., & Conger, S. 1994, ApJ, 436, L127

Neufeld, D. A., & Maloney, P. R. 1995, ApJ, 447, L17

Oliva, E., Salvati, M., Moorwood, A. F. M., & Marconi, A. 1994, A&A, 288, 457

Oliva, E., Marconi, A., Cimatti, A., Alighieri, & S. Di Serego 1998, A&A, 329, L21

Osterbrock, D. E., & Martel, A. 1993, ApJ, 414, 552

Peck, A. et al., 2001, Proc. IAU 206, eds. V. Migenes, E. Ludke, & M. Reid, in press.

Reid, M. J., & Moran, J. M. 1988, in Galactic & Extragalactic Radio Astronomy, 2nd ed., eds. G. L. Verschuur & K. I. Kellermann, (Berlin: Springer), 255

Reynolds, C. S., Nowak, M. A., & Maloney, P. R. 2000, ApJ, 540, 143

Risaliti, G., Elvis, M., & Nicastro, F. 2002, ApJ, 571, 234

Schinnerer, E., Eckart, A., Tacconi, L. J., Genzel, R., & Downes, D. 2000, ApJ, 533, 850

Trotter, A. S., Greenhill, L. J., Moran, J. M., Reid, M. J., Irwin, J. A., & Lo, K.-Y. 1998, ApJ, 495, 740

Veilleux, S., & Bland-Hawthorn, J., 1997 ApJ, 479, L105

Wallin, B. K., & Watson, W. D. 1997, ApJ, 476, 685

Wilson, A. S., Shopbell, P. L., Simpson, C., Storchi-Bergmann, T., Barbosa, F. K. B., & Ward, M. J. 2000, AJ, 120, 1325

Figure Captions

Fig. 1.— Maser spectra of total imaged power at two epochs and total power at one epoch. *(a)* 1998 June total imaged power. *(b)* 1997 July total imaged power (inverted and in gray). *(c)* 1995 total-power spectrum obtained with the Parkes antenna (taken from Greenhill et al., 1997). The instantaneous bandwidth of the VLBI observations was 400 km s^{-1} in 1997 and $\sim$ 600 km s^{-1} in 1998. The gray patches indicate velocities outside that range.

Fig. 2.— Sky distributions of H_2O maser emission in Circinus. Each symbol represents a single maser spot (i.e., emission in a single spectral channel). Color indicates heliocentric velocity as shown on the scale below, assuming the radio definition of Doppler shift. The horizontal black scale bar corresponds to 0.2 pc at a distance of 4.2 Mpc. *(a)* 1997 June 24. *(b)* 1997 July 25. *(c)* 1998 June 27 and 28. *(d)* 1997 July and 1998 June plotted together, registration is accurate to < 0.15 mas, based on the apparent alignment of emission clumps common to both epochs. The cross marks the estimated dynamical center of the disk (see Figure 3). The 1997 June data are excluded because of probable residual calibration errors that are probably responsible for the apparent elongation of many clumps of emission. In each map, the origin corresponds to $\alpha_{2000} = 14^h13^m09\overset{s}{.}95 \pm 0\overset{s}{.}02$, $\delta_{2000} = -65°20'21\overset{''}{.}2 \pm 0\overset{''}{.}1$. Error bars indicate uncertainties (1σ) in position, but in most cases they are smaller than the plotted symbols. The synthesized beams are shown symbolically in the lower left of each panel. For the epoch in 1998, there are different beams for the low-velocity and redshifted high-velocity data (red ellipse) and the blueshifted high-velocity data (blue ellipse).

Fig. 3.— Superposition of maps for 1997 July and 1998 June. Color indicates velocity, as in Figure 2. The black scale bar corresponds to 0.2 pc. The blue and red curves indicate the limb or midline of the putative edge-on warped disk, where the orbital velocity is parallel to the line of sight. The red curve is a second order polynomial fitted to the midline. The blue curve is a reflection of the polynomial about the center of the disk. The good agreement between the reflected curve and the blueshifted midline demonstrates how well the data fits an antisymmetric warp model. The lengths of the arcs indicate the range of radii over which redshifted maser spots trace a smoothly declining rotation curve (see Figure 4). The green line represents the innermost orbit, defined by the most highly red and blueshifted maser spots. The cross marks the estimated dynamical center of the disk.

Fig. 4.— Position-velocity diagrams combining data for 1997 July *(triangles)* and 1998 June *(circles)*. *(a)* Velocity plotted against impact parameter measured from the estimated position of the central engine. *(b)* Velocity plotted against cylindrical radius measured from the rotation axis of the innermost orbit of the proposed model disk. Both plots are presented because the orbital speed of disk material is a function of impact parameter while any rotation in the outflow is probably a function of cylindrical radius (see Kartje, Königl, & Elitzur 1999). Solid and dashed rotation curves reflect $v \propto r^{-0.5}$ and $v \propto r^{-0.45}$, respectively. The data points that lie close to these curves represent masers that arise close to the midline of the disk. The proposed wide-angle outflow is represented by the masers that lie inside and away from the two rotation curves. The steep diagonal

line delineates the locus for the innermost orbit.

Fig. 5.— Map for 1998 June where disk masers *(black)* are distinguished from outflow masers *(gray)*. Maser spots that lie more than 1 mas from the midline of the disk are considered to be outflow masers. The scale bar corresponds to 0.2 pc.

Fig. 6.— Total imaged power for 1998 June in which emission from the disk is shown in black. Other emission is shown in gray and is offset in flux density for clarity. The vertical line marks the systemic velocity. The spectrum for 1998 is shown because it is the best sampled overall. Outflow emission is offset up to $\sim \pm 160$ km s^{-1} from the systemic velocity. In 1997 July outflow emission was offset up to about -160 to $+190$ km s^{-1}.

Fig. 7.— Enlargement of the sky distribution of the H_2O maser spots associated with the putative outflow. The color scale is expanded, as shown by the scale bar, to indicate better the relationship of line-of-sight velocity and angular structure. The absence of obvious gradients indicates the emission does not originate in an organized rotating disk, however extreme the warp may be. The black scale bar corresponds to 0.2 pc.

Fig. 8.— Model of a thin, warped Keplerian accretion disk and the surface of a wide-angle bipolar outflow from the central engine. The disk has been tipped down at the front for clarity of perspective. Dots represent maser spots. Throughout, color indicates Dopper shift with respect to the systemic velicity, as in other figures. The warp of the disk shadows the surroundings, and maser emission appears only where there is a direct line of sight to the central engine. The location of the unshadowed region to the west is consistent with the know optical ionization cone (see, e.g., Veilleux & Bland-Hawthorn 1997). The case of Circinus appears to provide direct evidence that warped disks may determine the extent of ionization cones in AGN, as well as channel nuclear outflows, at least in some sources.

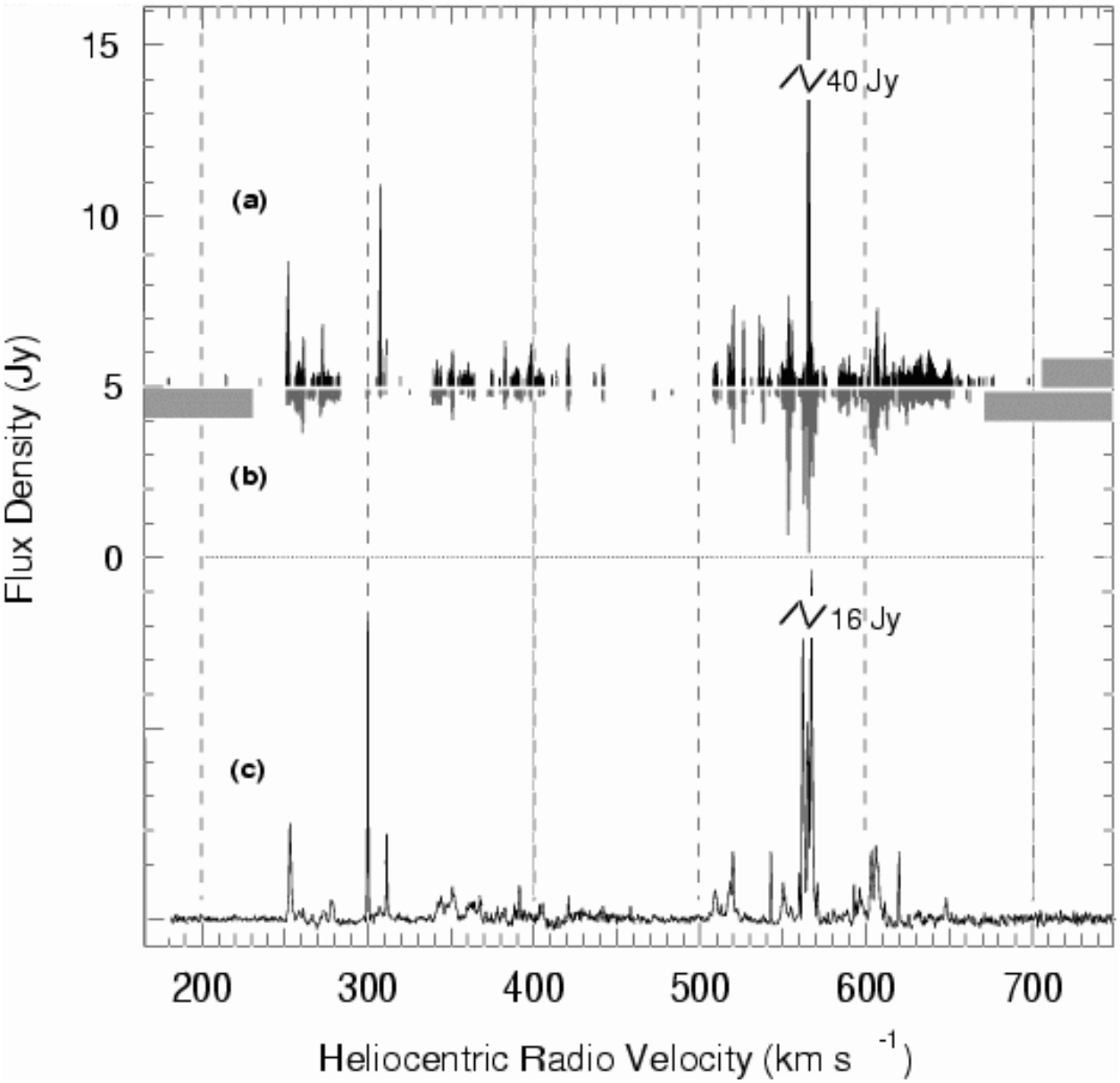

Fig. 1.— Greenhill et al.,

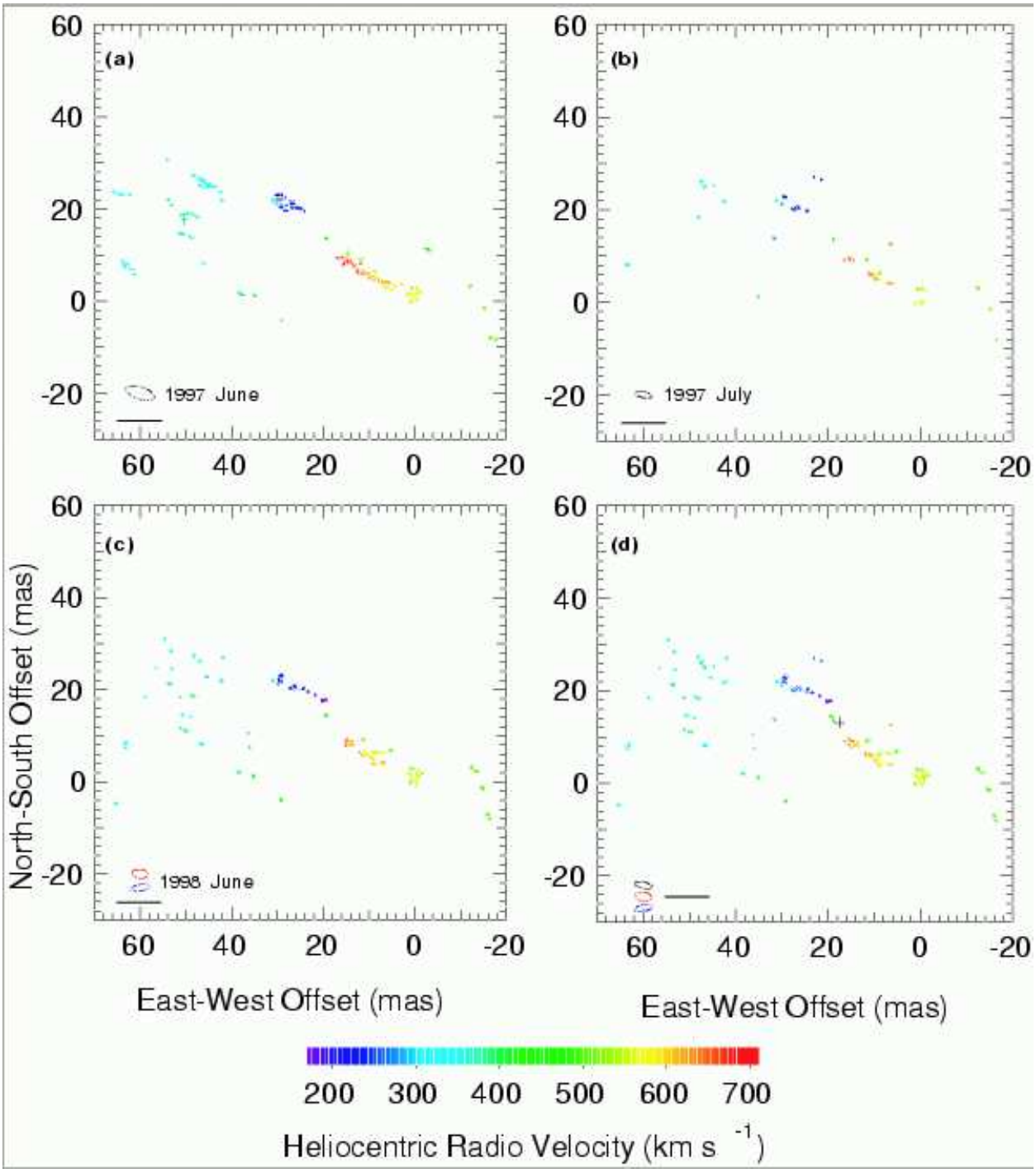

Fig. 2.— Greenhill et al.,

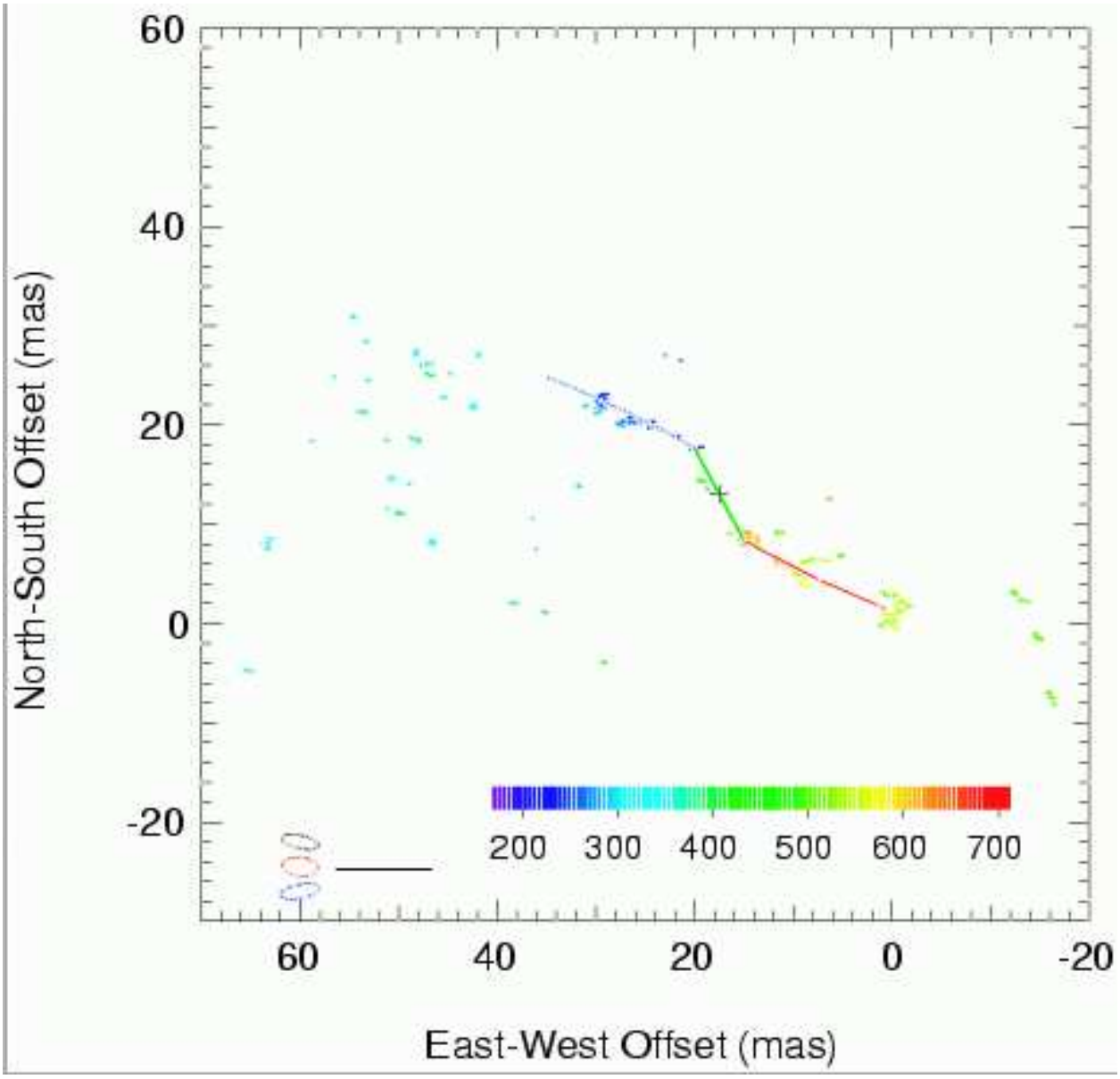

Fig. 3.— Greenhill et al.,

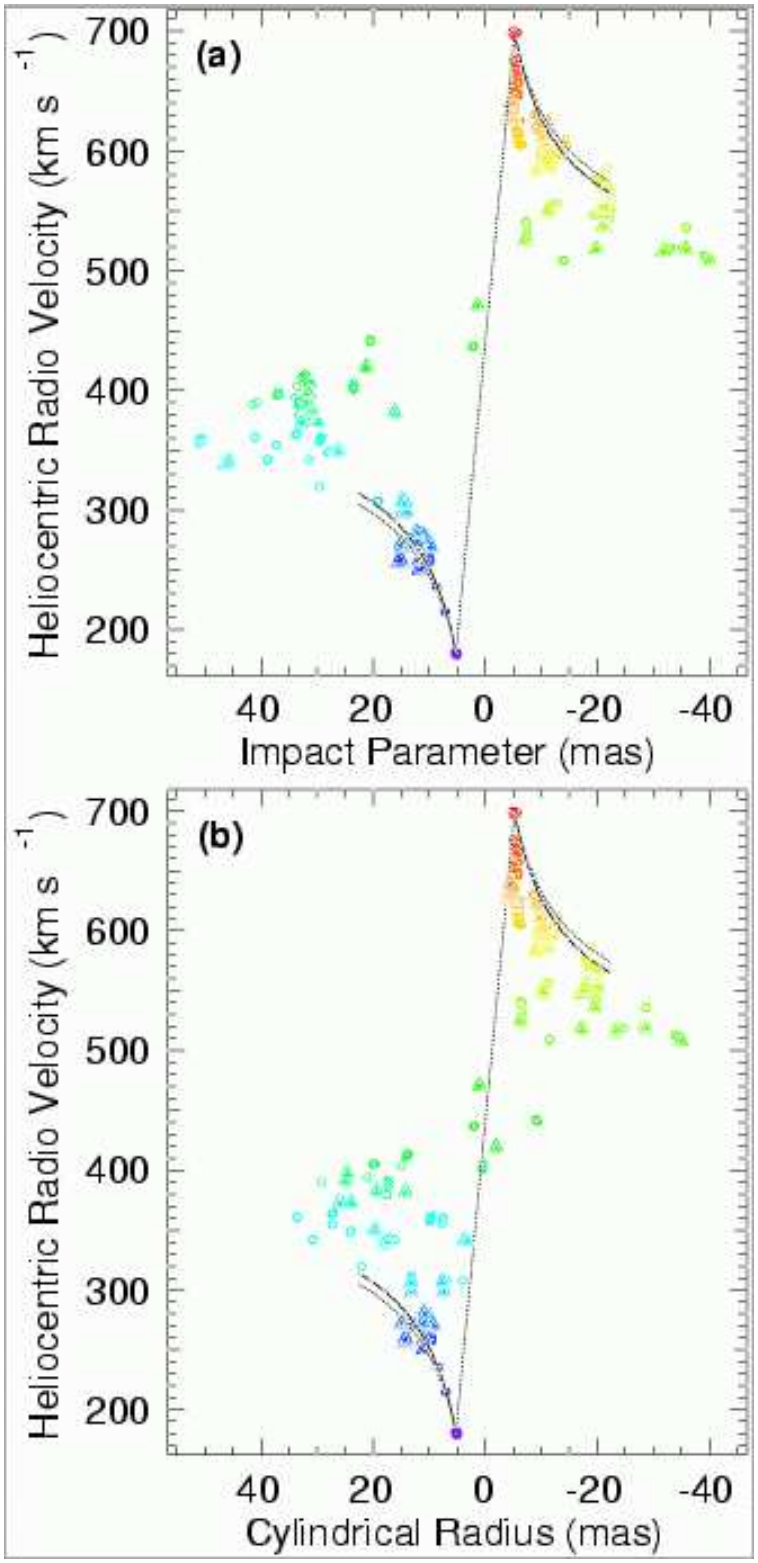

Fig. 4.— Greenhill et al.,

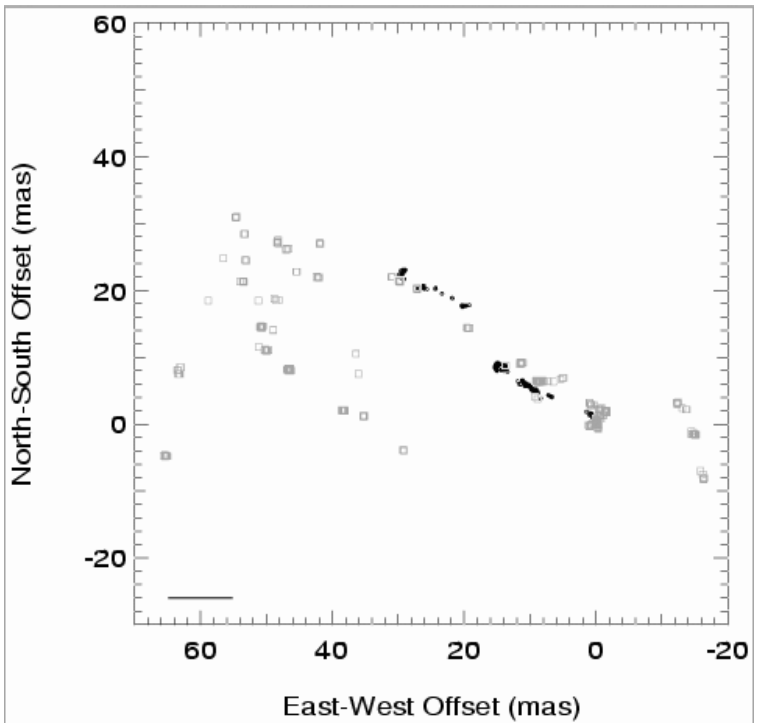

Fig. 5.— Greenhill et al.,

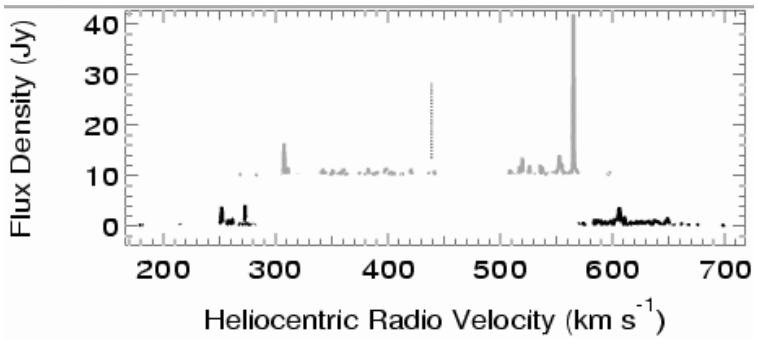

Fig. 6.— Greenhill et al.,

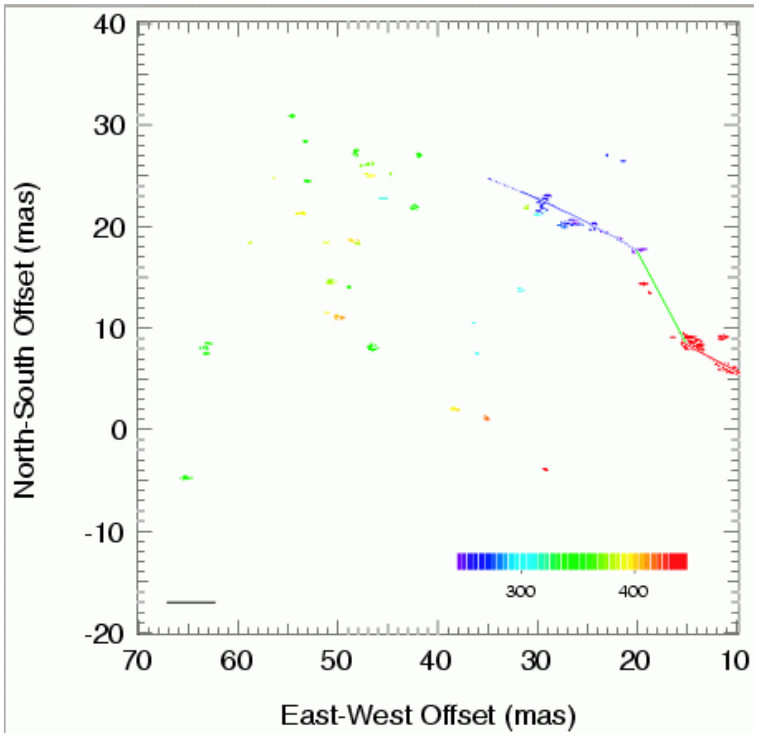

Fig. 7.— Greenhill et al.,

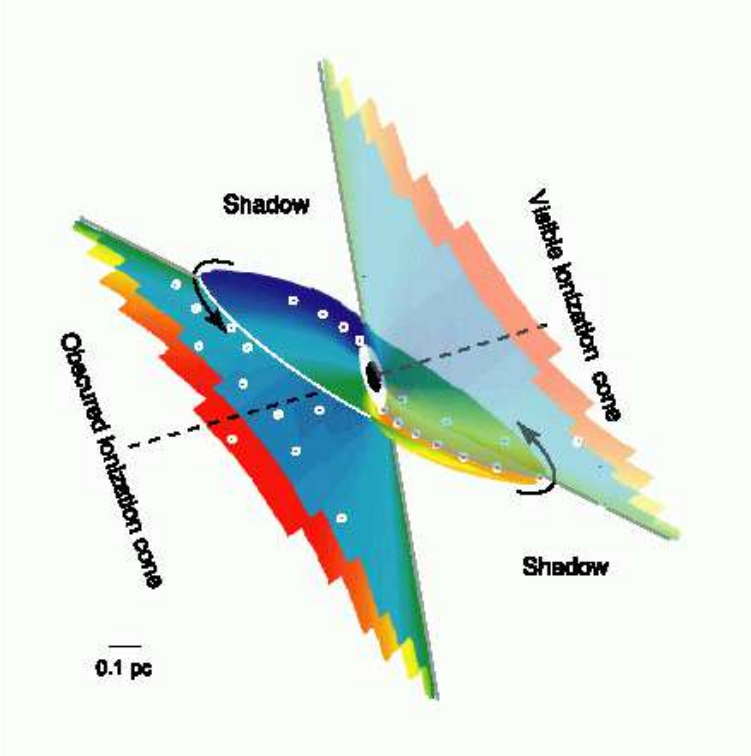

Fig. 8.— Greenhill et al.,